Korean Journal of Remote Sensing, Vol.23, No.5, 2007, pp.455~464

Adaptive Iterative Depeckling of SAR Imagery

Sang-Hoon Lee †

Kyungwon University

Abstract : Lee (2007) suggested the Point-Jacobian iteration MAP estimation (PJIMAP) for noise removal of the images that are corrupted by multiplicative speckle noise. It is to find a MAP estimation of noisy-free imagery based on a Bayesian model using the lognormal distribution for image intensity and an MRF for image texture. When the image intensity is logarithmically transformed, the speckle noise is approximately Gaussian additive noise, and it tends to a normal probability much faster than the intensity distribution. The MRF is incorporated into digital image analysis by viewing pixel types as states of molecules in a lattice-like physical system. In this study, the MAP estimation is computed by the Point-Jacobian iteration using adaptive parameters. At each iteration, the parameters related to the Bayesian model are adaptively estimated using the updated information. The results of the proposed scheme were compared to them of PJIMAP with SAR simulation data generated by the Monte Carlo method. The experiments demonstrated an improvement in relaxing speckle noise and estimating noise-free intensity by using the adaptive parameters for the Ponit-Jacobian iteration.

Key Words : SAR, Despeckling, Multiplicative Noise, Log-normal Distribution, MRF, MAP, Point-Jacobian Iteration, Adaptive Coefficients.

1. Introduction

Speckle noise due to wave coherence in Synthetic Aperture Radar (SAR) imagery is supposed to be dependent on the signal intensity in the sense that the noise level increases with the brightness. A simple statistical model of multiplicative noise (Dainty, 1984) has been often used for the speckle reduction. Many adaptive filters have been developed to reduce multiplicative noise in SAR images by taking local statistics. The best-known filters include the Lee filter (Lee, 1986), Frost filter (Frost *et al.*, 1982), Kuan filter (Kuan *et al.*, 1985) and Gamma filter (Lopez *et al.*, 1993). The Frost filter was designed as an adaptive Wiener filter that assumed an autoregressive exponential model for the scene reflectivity. Kuan considered a multiplicative speckle model and designed a linear filter based on the minimum mean-square error criterion, optimal when both the scene and the detected intensities are Gaussian distributed. The Lee filter was a particular case of the Kuan filter based on a linear approximation made for the multiplicative noise model. The Gamma filter was based on a Bayesian analysis of the image statistics where both intensity and speckle noise follow a Gamma distribution.

Received 8 October 2007; Accepted 22 October 2007.

† Corresponding Author: Sang-Hoon Lee (shl@kyungwon.ac.kr)

Lee (2007) suggested an iterative approach for despeckling the SAR images that are corrupted by multiplicative speckle noise. It is a *maximum a posteriori* (MAP) method using a Bayesian model based on the lognormal distribution for image intensity and a Markov random field (MRF) for image texture. When the image intensity is logarithmically transformed, the speckle noise becomes approximately Gaussian additive noise and it tends to a normal probability much faster than the intensity distribution (Arsenault and April, 1976). The MRF is incorporated into digital image analysis by viewing pixel type s as states of molecules in a lattice-like physical system defined on a Gibbs random field (GRF) (Georgii, 1979). Because of the MRF-GRF equivalence resulted from the Hammersley-Clifford theorem (Kindermann and Snell, 1982), the assignment of an energy function to the physical system determines its Gibbs measure, which is used to model molecular interactions. Thus, this assignment also determines the MRF. The MAP estimation of noisy-free imagery employs a Point-Jacobian iteration (Varga, 1962). The Point-Jacobian iteration MAP (PJIMAP) scheme was proved to yield much better results than the conventional approaches for the speckle reduction (Lee, 2007).

In this study, an adaptive scheme is proposed for the MAP estimation of Point-Jacobian iteration. Image processes are assumed to combine the random fields associated with intensity and texture respectively. The objective measure for determining the optimal restoration of this double compound stochastic image process is based on Bayes' theorem. The Bayesian model utilizes the parameters related to smoothing and bonding strength between neighbors. The smoothing parameter represents the relative strength of prior belief of spatial smoothness compared to observational information, and the bonding strength is represented by nonnegative coefficients associated with local texture model. In the new adaptive approach, the parameters are computed using the updated data at each iteration, while the PJIMAP uses the parameters estimated with the observation. The paper is organized as follows. Section 2 contains a description of the Bayesian model and the iterative MAP scheme, and the parameter estimation are presented in Sections 3. The experimental results of SAR simulation data including comparison with those of the PJIMAP are reported and discussed in Section 4. Finally, the conclusions are stated in Section 5.

2. Point-Jacobian Iteration MAP Estimation

A simple model of SAR imagery is usually given by

$$z_k \cong v_k \eta_k, k \in I_n \tag{1}$$

where $I_n = \{1, 2, \cdots, n\}$ is the index set of pixels of the image and $\{\eta_k\}$ are multiplicative noise following a log-normal distribution. If $Y = \{y_k = \ln z_k, k \in I_n\}$, $X = \{x_k = \ln v_k, k \in I_n\}$, and σ_k^2 is a variance of $\ln \eta_k$, then

$Y \sim N(X, \Sigma)$ where $\Sigma = diagonal\{\sigma_k^2, k \in I_n\}$.

Image processes are assumed to combine the random fields associated with intensity and texture respectively. The objective measure for determining the optimal restoration of this double compound stochastic image process is based on Bayes' theorem. Given an observed image Y, the Bayesian method is to find an MAP estimate from the mode of the posterior probability distribution of the noise-free vector X, or equivalently, to maximize the log-likelihood function

$$lPN = \ln P(Y|X) + \ln P(X). \tag{2}$$

The MRF is used to quantify the spatial interaction probabilistically, that is, to provide a type of prior information on the image texture. Due to the MRF-

GRF equivalence (Kindermann and Snell, 1982), an MRF is determined with a Gibbs measure. If R_i is the index set of neighbors of the ith pixel, $R = \{R_i \mid i \in I_n\}$ is a neighborhood system for I_n. A "clique" of $\{I_n, R\}$, c, is a subset of I_n such that every pair of distinct indices in c represents pixels which are mutual neighbors, and C denotes the set of all cliques. A GRF relative to the graph $\{I_n, R\}$ on X is defined as

$$P(X) = Z^{-1} \exp\{-E(X)\}$$
$$E(X) = \sum_{c \in C} V_c(X) \text{ (energy function)} \quad (3)$$

where Z is a normalizing constant and V_c is a potential function which has the property that it depends only on X and c. Specification of C and V_c is sufficient to formulate a Gibbs measure for the local texuture. A particular class of GRF, in which the energy function is expressed in terms of non-symmetric "pair-potentials," is used in this study (Kindermann and Snell, 1982). Here, the energy function of the GRF is specified as a quadratic function of X, which defines the probability structure of the texture process:

$$E_p(X) = \sum_{i \in I_n} \sum_{(i,j) \in C_p} \alpha_{ij}(x_i - x_j)^2 \quad (4)$$

where C_p is the pair-clique system and α_{ij} is a nonnegative coefficient which represents the bonding strength of the ith and the jth pixels.

The log-likelihood function of Eq. (2) using the log-normal intensity model and the GRF texture model is:

$$lPN \propto -(Y-X)'\Sigma^{-1}(Y-X) - X'\mathbf{B}X \quad (5)$$

where $\mathbf{B} = \{\beta_{ij}\}$ is the bonding strength matrix where

$$\beta_{ij} = \begin{cases} -\alpha_{ij} & \text{for } (i,j) \in C_p \\ \sum_{(i,j) \in C_p} \alpha_{ij} & \text{for } i = j. \\ 0 & \text{otherwise} \end{cases}$$

Since the log-likelihood function of Eq. (5) is convex, the MAP estimate of X is obtained by taking the first derivative:

$$\Sigma^{-1}(Y-X) - \mathbf{B}X = 0. \quad (6)$$

By solving Eq. (6) with the Point-Jacobian iteration (Varga, 1962), the noise-free intensity can be recovered iteratively (Lee, 2007): given an initial estimate, $\hat{x}_i^0$, at the hth iteration for $\forall i \in I_n$

$$\hat{x}_i^h = \frac{1}{\sigma_i^{-2} + \beta_{ii}} \left(\sigma_i^{-2} y_i - \sum_{(i,j) \in C_p} \beta_{ij} \hat{x}_j^{h-1} \right). \quad (7)$$

The iteration converges to a unique solution since $\gamma(\mathbf{M}_d^{-1}\mathbf{B}_s) < 1$ where $\gamma(\bullet)$denotes the spectral radius (Cullen, 1972) and

$$\mathbf{M}_d = diagonal\{\sigma_k^{-2} + \beta_{kk}, k \in I_n\}$$
$$\mathbf{B}_s = \{b_{ij} = \beta_{ij} \mid b_{ii} = 0\}$$

3. Adaptive Bonding Strength Coefficient Estimation

Various regions constituting an image can be characterized by textural components. The bonding strength coefficients of Eq. (4) are associated with local interaction between neighboring pixels and can provide some contextual information on the local region. It is important to choose the coefficients suitable for the analyzed image.

For the hth iteration, given the estimate of the previous iteration, $\hat{X}_{h-1} = \{\hat{x}_k^{h-1}, k \in I_n\}$, the posterior probability of X can be stated:

$$f(X \mid \hat{X}_{h-1}) \propto -(\hat{X}_{h-1} - X)'\Sigma^{-1}(\hat{X}_{h-1} - X) - X'\mathbf{B}X. \quad (8)$$

The MAP estimation of X is to find a mode of Eq. (8), and can be then considered as an optimization problem:

$$\underset{X}{\text{argmin}} \left\{ \sum_{i \in I_n} \sum_{(i,j) \in C_p} \alpha_{ij}(x_i - x_j)^2 \right\} \quad (9)$$
$$\text{subject to } \sigma_k^{-2}(\hat{x}_k^{h-1} - x_k)^2 < r, \ \forall k \in I_n$$

where r is a given constant related to the distribution of $\hat{X}_{h-1}$. The optimization of Eq. (9) can be rewritten as

$$\underset{X}{\operatorname{argmin}}\left\{\sum_{i\in I_n}\left[\phi_i \sum_{(i,j)\in C_p}\alpha_{ij}(x_i-x_j)^2+(\sigma_i^{-2}(\hat{x}_i^{h-1}-x_i)^2-r)\right]\right\} \quad (10)$$

and the coefficient $\beta_{ij} = -\phi_i\alpha_{ij}$ for $i \neq j$ and $\beta_{ii} = \phi_i$ can be estimated as in (Lee, 2007)

$$\hat{\alpha}_{ij}=\begin{cases}\dfrac{(\hat{x}_i^{h-1}-\hat{x}_j^{h-1})^{-2}}{\sum_{(i,k)\in C_p}(\hat{x}_i^{h-1}-\hat{x}_k^{h-1})^{-2}} & \text{for } (i,j)\in C_p \\ 0 & \text{otherwise}\end{cases}$$

$$\hat{\mu}_i=\frac{\sum_{k\in W_i}\hat{x}_k^{h-1}}{n_w} \quad (11)$$

$$\hat{\sigma}_i^2=\frac{\sum_{k\in W_i}(\hat{x}_k^{h-1}-\hat{\mu}_i)^{-2}}{n_w}$$

$$\hat{\phi}_i=\sqrt{\frac{r}{\hat{\sigma}_i^2\sum_{(i,k)\in C_p}\hat{\alpha}_{ik}(\hat{x}_i^{h-1}-\hat{x}_k^{h-1})^{-2}}}$$

where W_i is the index set of pixels belonging to the window centered on the ith pixel and n_w is the pixel number of W_i. W_i is a window defining the neighborhood system associated with C_p. In Eq. (10), $\{\phi_i\}$ and $\{\alpha_{ij}\}$ can be considered as the smoothing parameters of the relative strength of prior beliefs of spatial smoothness and the normalized bonding strength coefficients associated with a local texture model respectively. It is natural that the closer the pixels, the more the bonding strength between them. Under this supposition, the normalized bonding strength coefficient can be modified:

$$\hat{\alpha}_{ij}=\begin{cases}\dfrac{\pi_{ij}(\hat{x}_i^{h-1}-\hat{x}_j^{h-1})^{-2}}{\sum_{(i,k)\in C_p}\pi_{ik}(\hat{x}_i^{h-1}-\hat{x}_k^{h-1})^{-2}} & \text{for } (i,j)\in C_p \\ 0 & \text{otherwise}\end{cases} \quad (12)$$

where π_{ij} is a proximity coefficient proportional to the inverse of spatial distance between the ith and jth pixels. If one of the neighbor pixels has a very close value with the center pixel value compared to them of the other neighbor pixels, the coefficient associated with this neighbor pixel is very large relatively, and the contextual information of neighborhood is then dominated by this pixel, even if other neighbors have right information. This problem can be alleviated by giving a limitation on the quadratic distance of pixel pair in Eq. (12):

$$\hat{\alpha}_{ij}=\begin{cases}\dfrac{\pi_{ij}\delta_{ij}^{-2}}{\sum_{(i,k)\in C_p}\pi_{ik}\delta_{ik}^{-2}} & \text{for } (i,j)\in C_p \\ 0 & \text{otherwise}\end{cases} \quad (13)$$

where

$$\delta_{ij}^2=\max\{(\hat{x}_i^{h-1}-\hat{x}_j^{h-1})^2, k_\delta\hat{\sigma}_i^2\} \quad (14)$$

and k_δ is a predetermined constant.

4. Experiments

The results of the proposed adaptive iteration MAP (AIMAP) approach were compared to them of PJIMAP using simulation data generated by the Monte Carlo method.

If the number of scattering points per resolution cell is large in SAR, a fully developed speckle pattern can be modeled as the magnitude of a complex Gaussian field with independent and identically distributed real and imaginary components (Goodman, 1976). It leads to the Rayleigh distribution as the amplitude distribution model. For the experiment, 16-bit simulation SAR images with the Rayleigh distribution were generated using 3 patterns. The pattern images and the distribution of simulated noisy data used in this section are illustrated in Fig. 1. In this section, the graph of data distribution displays the frequency at intervals of 30. Patterns A and B have 5 classes and Pattern C has 4 class. Table 1 shows the mean intensity level and the number of pixels of each class.

For the Point-Jacobian iteration of Eq. (7), σ_i^2 is

Table 1. Mean Intensity Level and Number of Pixels of Classes of Simulation Patterns.

Class	Class Mean	Number of Pixels		
		Pattern A	Pattern B	Pattern C
1	500	143136	232560	262144
2	1000	191772	190708	262144
3	1500	164200	236432	262144
4	2000	278140	184796	262144
5	2500	271328	204080	

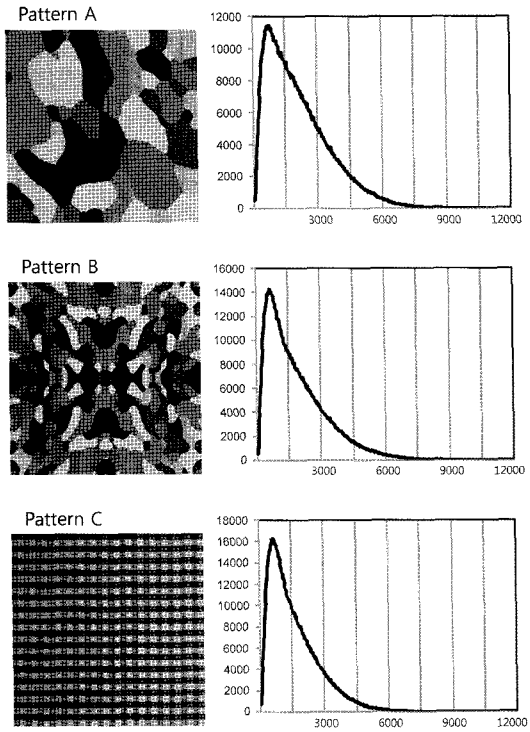

Fig. 1. Simulation image pattern and distribution of simulation data.

estimated using the observed intensities in the neighbor-window as in Eq. (11) :

$$\hat{\mu}_i = \frac{\sum_{k \in W_i} y_k}{n_w}$$
$$\hat{\sigma}_i^2 = \frac{\sum_{k \in W_i} (y_k - \hat{\mu}_i)^2}{n_w} \tag{15}$$

and the condition of convergence in Eq. (7) is defined as

$$\frac{\sum_{i \in I_n} \left| \hat{x}_i^{h-1} - \hat{x}_i^h \right|}{n} \le k_c \sqrt{\frac{\sum_{i \in I_n} \hat{\sigma}_i^2}{n}} \tag{16}$$

where $k_c << 1$ is a given constant. In the experiments, $\{\hat{\mu}_i\}$ were used for the initial estimates $\{\hat{x}_i^0\}$ and k was given with 0.01.

First the iteration MAP filters were applied to the simulation data of Pattern A using the neighborhood windows of 4 different sizes, 3×3, 5×5, 7×7 and 9×9. This experiment used $k_\delta = 1.0$ and $r = 1.0$. Table 2 contains the mean square errors of the despeckled data to the original noisy-free data:

$$MSE_{error} = \sqrt{\frac{\sum_{i \in I_n} (\hat{x}_i - \mu_i)^2}{n}} \tag{17}$$

where $\hat{x}_i$ and μ_i are the despeckled and original noisy-free values at the ith pixel respectively. Fig. 2 shows the distributions of the despeckled data resulted from PJIMAP and AIMAP. AIMAP yielded better results than PJIMAP in data distribution. As shown in Fig. 2, the despeckled data of PJIMAP using the windows of smaller sizes did not fit well to the distribution of original noisy-free data because the speckles of large value still remain in the resultant images. PJIMAP improved the speckle reduction in MSE_{error} and data distribution when using larger window. AIMAP also showed better performance in data distribution for lager windows, but did not always generate the despeckled data with smaller MSE_{error}. Fig. 3 shows the despeckled images resulted from PJIMAP and AIMAP using 9×9 window. This figure indicates that AIMAP can produce an image with much less speckles. Next, AIMAP was applied to the simulation data with different values of k_δ and r. The results contains in Table 3 and Fig. 4. As shown in Tables 2

Table 2. MSEerrors of despeckled Images Resulted from PJIMAP and AIMAP for Simulation Data of Pattern A.

Window Size	PJIMAP	AIMAP
3×3	345.22	178.59
5×5	229.61	163.44
7×7	202.42	168.01
9×9	198.66	177.37

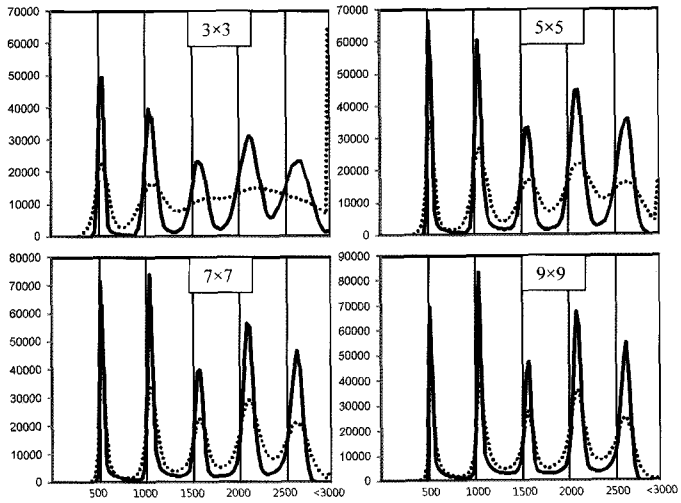

Fig. 2. Distributions of despeckled data of PJIMAP (dots) and AIMAP for simulation data of Pattern A.

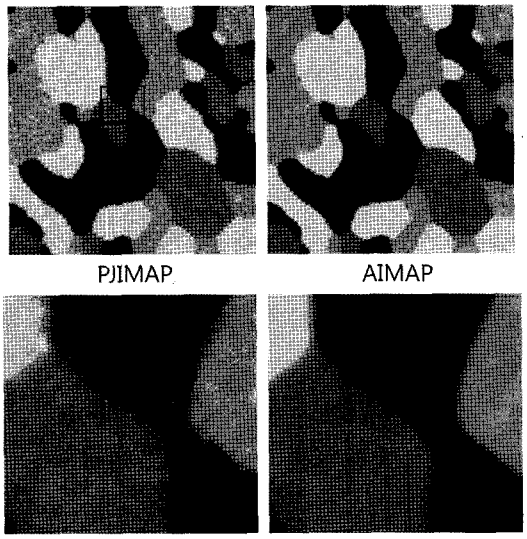

Fig. 3. Despeckled images of PJIMAP and AIMAP using 7×7 window (2nd row: enlarged images of sub area).

Table 3. MSE_{error}s of Despeckled Images Resulted from AIMAP with Different Given Constants for Simulation Data of Pattern A.

Window Size	$k_\delta = 0.1, r = 1.0$	$k_\delta = 1.0, r = 25.0$
3×3	276.64	178.34
5×5	190.35	164.37
7×7	170.28	169.30
9×9	164.82	179.19

and 3, the value of r did not give an effect on the performance, but the filter generated different result for different k_δ. When using small value of k_δ, the smaller the MSE_{error}, the larger the window size, as in the results of PJIMAP. Fig. 4 shows that the smaller value of k_δ resulted in producing the image with worse fit in data distribution.

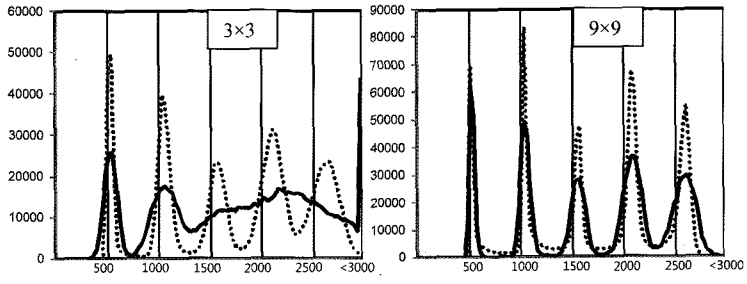

Fig. 4. Distributions of despeckled data of AIMAP with k_δ = 0.1 and 1.0 (dots) using windows of 3×3 and 9×9 for simulation data of Pattern A.

Table 4. MSE_{error}s of despeckled Images Resulted from PJIMAP and AIMAP for Simulation Data of Pattern B.

Window Size	PJIMAP	AIMAP
3×3	321.43	192.74
5×5	241.43	209.94
7×7	241.98	238.00
9×9	267.96	269.69

AIMAP was applied to the simulation data of more complex patterns. Table 4 contains the MSE_{error} results of PJIMAP and AIMAP using 4 different window sizes with k_δ = 1.0, r = 1.0 for simulation data of Pattern B. Fig. 5 displays the data distribution of despeckled images resulted from PJIMAP and AIMAP. The results of Table 4 and Fig. 5 indicate that AIMAP performs better for the speckle reduction than PJIMAP. When AIMAP was applied to the data with k_δ = 0.1 using 7×7 window, the MSE_{error} of k_δ = 0.1 is 193.44, while the error of k_δ = 1.0 is 238.00. However, Fig. 6 shows that the larger value of k_δ generated the despeckled data fitting a little better to the data distribution. As shown in Table 4, AIMAP produced smaller MSE_{error}s with smaller windows. The experiments of different values of r showed that the r values also have little effect on the results. It may demonstrate that AIMAP of small k_δ and window is more proper for the data with Pattern B contrary to the case of Pattern A. Fig. 7 illustrates the despeckled images generated from AIMAP. It shows that when using large window, AIMAP performs

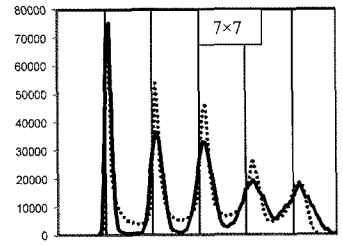

Fig. 6. Distributions of despeckled data of AIMAP with k_δ = 0.1 and 1.0 (dots) using windows of 7×7 for simulation data of Pattern B.

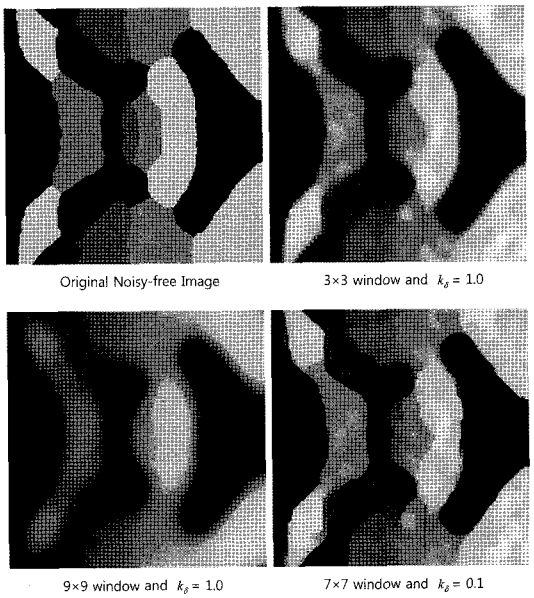

Fig. 7. Despeckled images of sub-area resulted from AIMAP for simulation data of Pattern B.

well in despeckling the data of inner area of large regions, but it results in improper smoothing in the boundary area of small regions. The 4th image

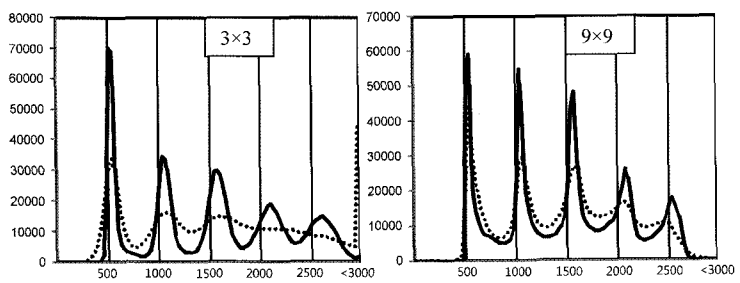

Fig. 5. Distributions of despeckled data of PJIMAP (dots) and AIMAP using windows of 3×3 and 9×9 for simulation data of Pattern B.

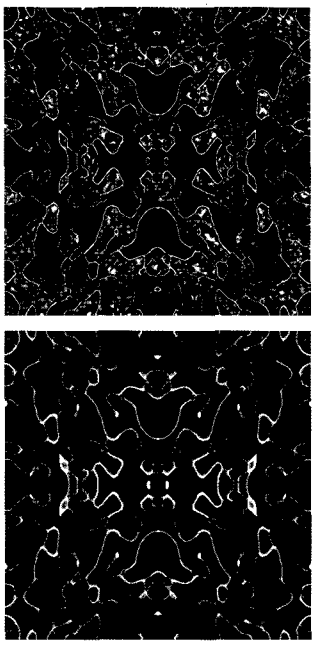

Fig. 8. Error images of despeckled data resulted from AIMAP of 3×3 (1st row) and 9×9 windows.

Table 5. MSE_{error}s of despeckled Images Resulted from PJIMAP and AIMAP for Simulation Data of Pattern C.

Window Size	PJIMAP	AIMAP
3×3	268.19	168.12
5×5	210.00	194.43
7×7	222.03	224.68
9×9	254.31	267.96

(south-east corner) shows the effect of small k_δ, which makes the filter estimate the noisy-free image using more information of neighbors with similar values. Fig. 8 displays the error images, $\{(\hat{x}_i - \mu_i)^2, i \in I_n\}$ of despeckled data generated from AIMAP. This error images clearly shows that the large window is better in the inner area and the small window is better in the boundary area. Table 5 and

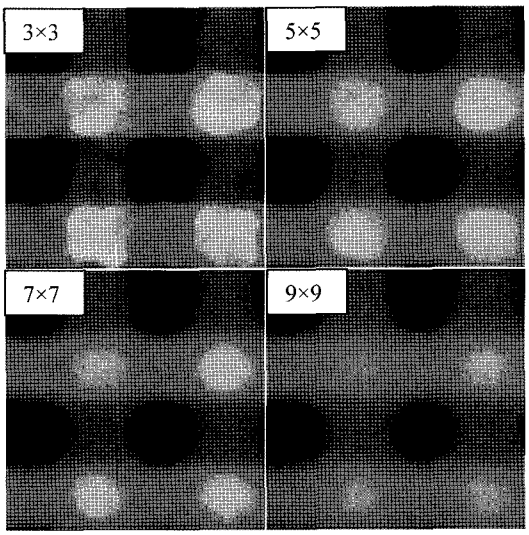

Fig. 10. Despeckled images of sub-area resulted from AIMAP for simulation data of Pattern C with 4 different window sizes.

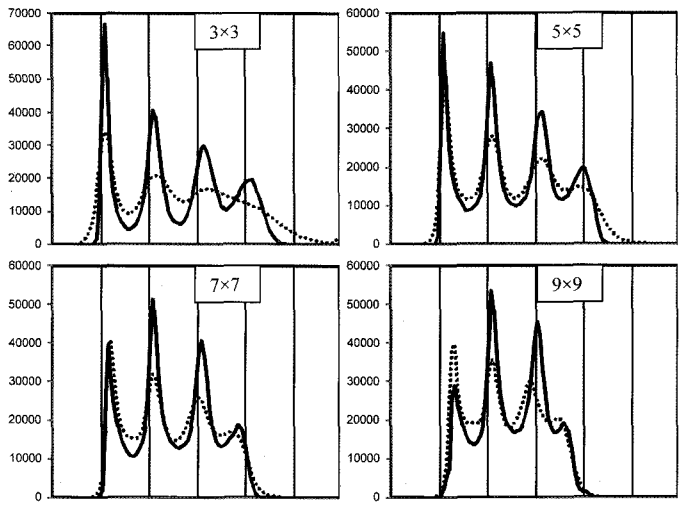

Fig. 9. Distributions of despeckled data of PJIMAP (dots) and AIMAP for simulation data of Pattern C.

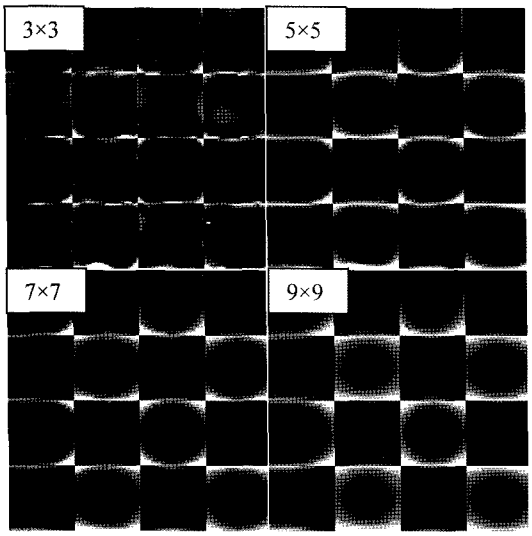

Fig. 11. Error images of despeckled images of Fig. 10.

Figs. 9 - 11 contains the results of AIMAP for the simulation data of Pattern C. These results also shows the similar problem.

6. Conclusions

Lee (2007) proposed PJIMAP filter for despeckling SAR imagery, which is an iterative approach using a Bayesian model to find MAP estimation of noise-free intensity. The algorithm is established based on a multiplicative noise model using a log-normal distribution and a texture model using MRF. PJIMAP demonstrated the potentiality to relax speckle noise and estimate noise-free intensity. The Bayesian model based on double compound stochastic image process utilizes the smoothing parameter that represents the relative strength of prior beliefs of spatial smoothness compared to information on the observation and the bonding strength coefficients associated with a local texture model. The proposed approach adaptively estimates the Bayesian parameters from the updated data at each iteration, while the PJIMAP uses the parameters estimated with the observation. The new scheme was extensively evaluated using SAR simulation data by comparing the results with them of PJIMAP. The experimental results show an improvement in speckle reduction by using the adaptive parameters for the Ponit-Jacobian iteration. However, the new approach still has a problem in determining a proper size of window related to the neighborhood system of local texture model. The use of large window results in improper smoothing in the boundary area of small regions. A larger window smoothes the image to some extent and results in fading the detailed features existed in the scene.

References

Arsenault H. H. and G. April, 1976. Properties of speckle integrated with a finite aperture and logarithmically transformed, *J. Opt. Soc. Amer.*, 66: 1160-1163.

Cullen, C. G., 1972. *Matrices and Linear Transformations*. Reading, MA: Addison-Wesley.

Dainty, J. C., 1984. *Laser Speckle and Related Phenomena*, Second Enlarged Edition.

Frost, V. S., J. A. Stiles, K. S. Shanmugan, and J. C. Holtzman, 1982. A model for radar images and its application to adaptive digital filtering of multiplicative noise, *IEEE Trans. Pattern Anal. Mach. Intell.*, 4: 157-165.

Georgii, H. O., 1979. *Canonical Gibbs Measure*. Berlin, Germany: Springer-Verlag.

Goodman, J. W., 1976. Some fundamental properties of speckle, *J. Opt. Soc. Amer.*, 66: 1145-1150.

Kuan, D. T., A. A. Sawchuk, and P. Chavel, 1985. Adaptive noise smoothing filter for images with signal-dependent noise, *IEEE Trans. Pattern Anal. Machine Intell.*, 7: 165-177.

Kindermann R. and J. L. Snell, 1982. *Markov Random Fields and Their Application*, Providence, R.I.: Amer. Math. Soc.

Lee, J. S., 1986. Speckle suppression and analysis for synthetic aperture radar, *Optical Engineering*, 25: 656-643.

Lee, S-H., 2007. Speckle Removal of SAR Imagery Using a Point-Jacobian Iteration MAP Estimation, *Korean Journal of Remote Sensing*, 23: 33-42.

Lopes, A., E. Nezry, R. Touzi, and H. Laur, 1993. Structure detection and statistical adaptive speckle in SAR images, *International Journal of Remote Sensing*, 13: 1735-1758.

Varga, R. S., 1962. *Matrix Iterative Analysis*, Englewood Cliffs, NJ: Prentice-Hall.